



HAL
open science

Supercritical carbon dioxide solubility measurement and modelling for effective size reduction of nifedipine particles for transdermal application

Thibault Massias, Suenia de Paiva Lacerda, Jacqueline Resende de Azevedo, Jean-jacques Letourneau, Marie-Alexandrine Bolzinger, Fabienne Espitalier

► To cite this version:

Thibault Massias, Suenia de Paiva Lacerda, Jacqueline Resende de Azevedo, Jean-jacques Letourneau, Marie-Alexandrine Bolzinger, et al.. Supercritical carbon dioxide solubility measurement and modelling for effective size reduction of nifedipine particles for transdermal application. *International Journal of Pharmaceutics*, 2023, 630, pp.122425. 10.1016/j.ijpharm.2022.122425 . hal-03875943

HAL Id: hal-03875943

<https://imt-mines-albi.hal.science/hal-03875943>

Submitted on 19 Dec 2022

HAL is a multi-disciplinary open access archive for the deposit and dissemination of scientific research documents, whether they are published or not. The documents may come from teaching and research institutions in France or abroad, or from public or private research centers.

L'archive ouverte pluridisciplinaire **HAL**, est destinée au dépôt et à la diffusion de documents scientifiques de niveau recherche, publiés ou non, émanant des établissements d'enseignement et de recherche français ou étrangers, des laboratoires publics ou privés.

Supercritical carbon dioxide solubility measurement and modelling for effective size reduction of nifedipine particles for transdermal application

Thibault Massias^{a,b}, Suênia de Paiva Lacerda^a, Jacqueline Resende de Azevedo^b, Jean-Jacques Letourneau^a, Marie-Alexandrine Bolzinger^b, Fabienne Espitalier^{a,*}

^a Centre RAPSODEE, IMT Mines-Albi, UMR CNRS 5302, Université de Toulouse, Albi, France

^b Laboratoire d'Automatique, de Génie des Procédés et de Génie Pharmaceutique, (LAGEPP UMR CNRS 5007), Université Claude Bernard Lyon 1, Villeurbanne, France

A B S T R A C T

Nifedipine (NIF) is a Class II drug of the Biopharmaceutical Classification System (BCS) with low oral bioavailability, low dissolution rate and significant hepatic drug metabolism. The transdermal route using supersaturated systems could be considered. For this purpose, physicochemical properties of NIF such as its dissolution rate, may be a limiting factor and must be improved. Crystallization processes assisted by supercritical carbon dioxide (scCO₂) and particularly the Rapid Expansion of Supercritical Solution (RESS) process may improve drug bioavailability by reducing particle size and consequently increasing surface area. This study addresses the reduction of NIF particle size using scCO₂-RESS as crystallization process. Experimental solubility studies were performed at different temperature (308 and 318 K) and pressure ranges (9–24 MPa). Solubility data were correlated with two thermodynamic models in order to predict NIF solubility in scCO₂. Optimized operating conditions, identified by thermodynamic modelling, allowed the production of thinner NIF particles and a size reduction up to ten fold. Particle size reduction improved NIF dissolution kinetics in aqueous medium: after 90 min, 42 % of raw NIF was released against 80 % for crystallized NIF. The scCO₂-RESS process is a solvent free process, that can produce micronized or nanosized crystals able to improve physicochemical properties of poorly water-soluble drugs.

1. Introduction

Nifedipine (NIF) is a calcium channel blocker prescribed for the treatment of hypertension and for the prevention of angina pectoris (Godfraind, 2017). NIF is an active pharmaceutical ingredient (API) belonging to Class II of the Biopharmaceutical Classification System (BCS), characterized by a low aqueous solubility and a high permeability (Amidon et al., 1995; Horster, 1975), but undergoes pronounced first-pass effects, resulting in a limited oral bioavailability ranging between 35 and 77% (Echizen and Eichelbaum, 1986; Foster et al., 1983; Raemisch and Sommer, 1983; Waller et al., 1984). Oral bioavailability of NIF is limited because of its low aqueous solubility, low dissolution rate and significant hepatic drug metabolism. Various strategies could be investigated to overcome this limited bioavailability: *i*) administration of higher doses to patients to overcome solubility and dissolution issues, thereby increasing pre-existing side effects; *ii*) use of drug delivery systems such as polymeric nanoparticles, but expensive to produce and

frequently associated to toxicological issues (Sharma et al., 2012); *iii*) alternative routes of administration, such as the transdermal route in order to avoid the gastrointestinal first-pass metabolism (Khan and Roberts, 2018; Moser et al., 2001b). The choice of the transdermal route is suitable provided that the drug has a low molecular weight, a high solubility in pharmaceutical ingredients and a good skin permeability (Bolzinger et al., 2012; Hadgraft and Lane, 2016). However, to deliver the therapeutic dose of NIF by transdermal route, slow dissolution rate associated with low solubility are limiting factors.

In this context, particle engineering technologies are an interesting approach to improve the physicochemical properties of APIs such as solubility, dissolution rate and particle size reduction (Bolten and Türk, 2012; Chen et al., 2018; Xu and Luo, 2014). These processes are intended to increase the bioavailability of poorly water-soluble drugs in supersaturated systems (Henmi et al., 1994). Supersaturation in the dosage form is the driving force that may enhance NIF transdermal flux. A supersaturated system is based on the increase of the saturation degree of

* Corresponding author at: RAPSODEE, Research Centre in Albi on Particulate Solids, The Energy and Environment, UMR CNRS 5302, IMT Mines-Albi, France.
E-mail address: fabienne.espitalier@mines-albi.fr (F. Espitalier).

the drug in the vehicle and has been widely used to formulate transdermal systems (Moser et al., 2001b). Various methods have been reported to create a supersaturated state for transdermal administration such as application of water free vehicle under occlusion. The hydration coming from the Trans Epidermal Water Loss (TEWL, $\text{g}\cdot\text{m}^{-2}\cdot\text{h}^{-1}$) increases the skin water content and decreases the solubility of the loaded drug vehicle leading to a supersaturated system (Kemken et al., 1992). The technique of solvent evaporation (Parhi and Swain, 2018; Santos et al., 2012), mixing with co-solvent (Megrab et al., 1995; Moser et al., 2001a) or changing the temperature could also overcome driving force issues.

Particle size reduction, leading to an improvement of dissolution rate, could be achieved using top-down (reduction of the initial powder) or bottom-up (crystallization after dissolution) approaches. For NIF top-down approach, combination of high shear mixing, high pressure homogenization and spray drying for the production of dried NIF particles associated with additives showed an improvement of physicochemical properties (Hecq et al., 2005). Co-grinding NIF associated with chitosan also showed an improvement of dissolution kinetics (Portero et al., 1998). Among bottom-up approaches, NIF crystallization through spray-drying process for solid dispersion production has also been studied (Soulaïrol et al., 2015). At present, improvement of NIF physicochemical properties have mostly been done using high energy consumption processes associated with organic solvents and additives. Considering the need to reduce energy consumption, the use of organic solvent and/or additives, green chemistry processes for safer particle generation could be a good option.

In that context, supercritical CO_2 (scCO_2)-assisted processes, have gained considerable importance as green chemistry processes, in the pharmaceutical, cosmetic and food fields (Badens et al., 2018). They have been widely used as particle micronization or nanonization processes with a narrow size distribution (Fages et al., 2004; Padrela et al., 2018). Particle size reduction leads to an increase in the specific surface area and consequently to higher dissolution rates. Supercritical CO_2 processes mainly use CO_2 as a solvent (Rapid Expansion of Supercritical Solution (RESS) and related processes), as an anti-solvent (Supercritical anti-Solvent (SAS) and related processes) (Djerafi et al., 2015; Montes et al., 2012; Won et al., 2005) or as an additive (Particle from Gas Saturated Solution (PGSS) and related processes) (Pestieau et al., 2015). Well documented literature reviews defined these different processes as promising methods to improve bioavailability of poorly water soluble drugs (Franco and De Marco, 2021; Padrela et al., 2018).

In this study, RESS process was chosen to produce micronized NIF as it is able to perform drug particle size reduction without using organic solvent, as reported in previous works (Fang et al., 2020; Su et al., 2009; Türk and Bolten, 2016). In order to generate small particles, the operating conditions must be well defined to achieve high supersaturation values to ensure drug crystallization and suitable particle yield and size. To design and develop optimized scCO_2 -RESS process parameters, API equilibrium concentration in scCO_2 should be determined at first. Solubility data, when combined with thermodynamic modelling, enable predicting drug solubility in scCO_2 at different temperature and pressure conditions. The most efficient experimental parameter could therefore be selected.

In the present work, NIF experimental solubility in scCO_2 is reported at 308 and 318 K for pressures ranging between 9 and 24 MPa. Thermodynamic modelling applications were performed using solubilities from this work and literature. Operating conditions were identified from predicted crystallization driving force for an effective NIF size

reduction compared to raw NIF. Then, NIF particles have been generated using scCO_2 -RESS process and characterized by particle size distribution, powder crystallinity and dissolution kinetics at the skin temperature of 32 °C (305.15 K) for topical application.

2. Materials and methods

2.1. Materials

NIF (99 wt% purity) was purchased from LEAP Chem (China). Absolute ethanol, sodium chloride (≥ 98 wt% purity), HPLC grade acetonitrile and methanol (≥ 99.9 wt% purity) were acquired from VWR Chemicals (France). Polysorbate 20 was provided by Croda (France). Supercritical CO_2 apparatus for processing samples was purchased from Separex (France). High CO_2 purity (≥ 99.7 % purity) was provided by Linde (France).

2.2. Methods

2.2.1. NIF HPLC analysis

As NIF is a light-sensitive drug (Grundty et al., 1994), all experiments were conducted in the dark. The HPLC system (1260 Infinity, Agilent France) was composed of a reversed phase column ProntoSIL Eurobond C18 (150 mm \times 4.6 mm, 5 μm) and an UV detector set at 238 nm. The mobile phase was acetonitrile/methanol/water (15/30/55; v/v) for 10 min, followed by acetonitrile/methanol/water (15/55/30; v/v) to eluate NIF for 20 min. This gradient method was developed to separate NIF from its degradation products. The injection volume was 15 μL , and the flow rate was 0.7 mL/min for a retention time of 21.8 min.

2.2.2. Solubility measurement in pure scCO_2

A continuous flow apparatus (Sauceau et al., 2000) was used to perform solubility measurements in scCO_2 (Fig. 1). The experimental setup consisted in three main parts: (1) a CO_2 supply system; (2) a system including the solid and (3) a system to recover the solute dissolved in CO_2 . In the first element (1), a high-pressure pump (ISCO, 500D; P), was used for CO_2 circulation through the second system (2) at constant pressure and a heat exchanger (H) was used to preheat the CO_2 . The second system was a temperature-controlled environmental chamber (TO) comprising a heat exchanger (H), a cell containing the solid (C), a 6-way valve and an expansion valve. A flow rate lower than 1 mL/min ensured that the scCO_2 was saturated at the outlet of the cell. Once saturated, the scCO_2 reached the third component of the device. In this part (3), the mixture CO_2 -solute was mixed with ethanol and was expanded. After mixing and expansion, the fluid was directed to a temperature-controlled stirred tank (V) at 278.15 K. In this atmospheric pressure vessel, the gaseous CO_2 separates naturally from the mixture. The ethanol and the solute circulate in a closed loop by means of a peristaltic pump (PP). Approximately 3 g of NIF was introduced into the cell. The total volume of CO_2 was measured by means of a gas volumeter (G) placed at the vessel. To optimise the measurement, a fixed temperature was used into the system while pressure was modified every 10 to 20 min after sampling into the ethanol stream and measuring the gasometer value. Samples are collected regularly from the stirred tank. The cumulated drug concentration in the liquid phase was analysed by HPLC (Fig. S1). Finally, the extracted mass fraction at defined temperature and pressure was calculated from Equation (Eq (1)).

$$w_{\text{eqNIF}}(P; T) = \frac{C_{\text{NIF}} \times (m_{\text{EtOH initial}} - \sum m_{\text{EtOH samples}})}{C_{\text{NIF}} \times (m_{\text{EtOH initial}} - \sum m_{\text{EtOH samples}}) + ((V_{\text{CO}_2} - V_{\text{CO}_2 \text{ sample } n-1}) \times \rho_{\text{CO}_2, 20^\circ \text{C}, 1 \text{atm}})} \quad (1)$$

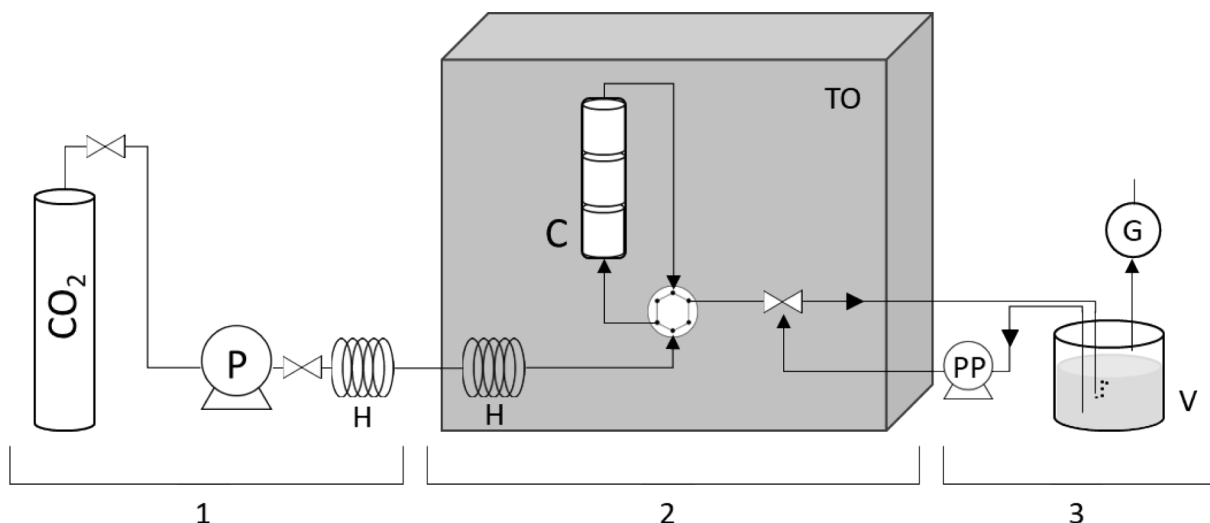


Fig. 1. Schematic representation of solubility apparatus. (1) CO₂ supply system; (2) solid inclusion system; (3) solute recovery system. (P) pump; (H) heaters; (C) equilibrium cell; (TO) thermostatic oven; (PP) peristaltic pump; (V) vessel; (G) gasometer.

where, C_{NIF} ($\mu\text{g/g}$) is determined by HPLC, m_{EtOH} samples (g) is the amount of EtOH solution sampled from the vessel for HPLC analysis. V_{CO_2} is expressed in m^3 and the density ρ in kg/m^3 . All experiments were carried out in triplicate.

2.2.3. Thermodynamic modelling

Equilibrium concentrations of NIF in scCO_2 were necessary to understand extraction and crystallization processes. More specifically, accurate prediction of equilibrium concentration for difficult experimental measurement conditions (*i.e.* low and high pressures) was required to define operating conditions of the process.

In this work, two models were chosen to describe experimental data: Chrastil's density-based model and Peng Robinson's Equation of State model (PR-EoS). Extrapolation from modelling application was used to determine supersaturation ratio (S) which is defined by the ratio of fugacity (Eq. (2)).

$$S = \frac{f_{NIF}}{f_{NIF, \text{equil}}} \quad (2)$$

Where S is a fugacity ratio at a same temperature and pressure. This ratio corresponds to the fugacity before the crystallization at non-equilibrium composition, and the fugacity at equilibrium composition.

2.2.3.1. Chrastil's density-based model. The Chrastil's model is a semi-empirical model. Its equation relates the solubility of a compound to the density of the mixture (Chrastil, 1982). Moreover, these equations are based on a solvato-complex between solute and solvent. These models are therefore suitable for polar active ingredients in solid form. Chrastil's density-based correlation model was used to validate NIF solubility measurement in scCO_2 (Eq. (3)).

$$\ln(y_{NIF}) = a \ln(\rho_{\text{solvent}}(T, P)) + \frac{b}{T} + c \quad (3)$$

Where c is the molar fraction solubility conditions in scCO_2 (n/n) for the reference density and temperature of the gas, b corresponds to $\Delta H^*/RT$ with R the molar gas constant and, ΔH^* the energy value close to that required to promote a phase change solid to solution and the formation of a solvato-complex between solvent and solute. a is the association number (*i.e.*, the number of solvent molecules necessary for a molecule of solute to create the solvato-complex).

2.2.3.2. Peng Robinson's equation of state model (PR-EoS). Equation of state models (EoS), such as PR-EoS, predict solubility by relating

pressure, temperature and molar volume (Peng and Robinson, 1976) (Eq. (4)). PR-EoS model is a classical cubic equation model based on the competition of repulsive and attractive forces between molecules in a mixture. Through the knowledge of the sublimation pressure of solids, the fugacity is calculated to predict the equilibrium. PR-EoS model allows a more accurate description of the equilibrium concentration in gas phase and has therefore been used for this purpose.

$$P = \frac{R \cdot T}{v - b} - \frac{a}{v^2 + 2bv - b^2} \quad (4)$$

where P is the pressure expressed in MPa, R is the universal gas constant, T is the temperature in K, v is the molar volume in $\text{m}^3 \cdot \text{mol}^{-1}$, a and b refers to attractive and repulsive interactions, respectively. The fitting model parameters are the critical temperature $T_{c,NIF}$, the critical pressure $P_{c,NIF}$, the acentric factor ω_{NIF} for the pure NIF, and binary interaction parameters (k_{12} and l_{12} of the van der Waals mixing rule) for the binary system CO_2 -NIF. Data fitting consists in finding values of these five parameters that minimize the criteria equals to the sum of the squared errors, which are the difference between the 34 reconciliated experimental data and there corresponding model values. The Nelder-Mead simplex algorithm as described in Lagarias et al. (1998) has been used to determine optimized parameters values.

2.2.4. Solid generation

The crystallization apparatus, previously described in literature (Rodier et al., 2005), is presented in Fig. 2. Briefly, liquid CO_2 was pumped to reach the set pressure (Fig. 2, A). Then CO_2 was subsequently heated to the supercritical region (B), and the scCO_2 percolated through the solid (*i.e.*, raw NIF) stored in the extraction autoclave (C; T_1, P_1). The process parameters are detailed on Table 1. The CO_2 -NIF mixture was sprayed through a nozzle into the expansion vessel (D). In this autoclave, the operating conditions were chosen to keep the CO_2 in a gaseous phase (T_2, P_2). The CO_2 was subsequently recycled at the exit of this autoclave.

2.2.5. Physicochemical and morphological characterizations

2.2.5.1. Particle size distribution. Particle size analysis were performed using a Mastersizer 3000 equipment (Malvern Panalytical, France). Powders were dispersed at approximately 10 mg/g in distilled water. Then, a sufficient amount of dispersion was injected to the equipment cell (100 mL of water) to obtain an obscuration signal between 1 and 30 %. Injected suspensions were sonicated during 150 s (40 W, 40 kHz) using the instrument internal system. Each analysis was conducted twice

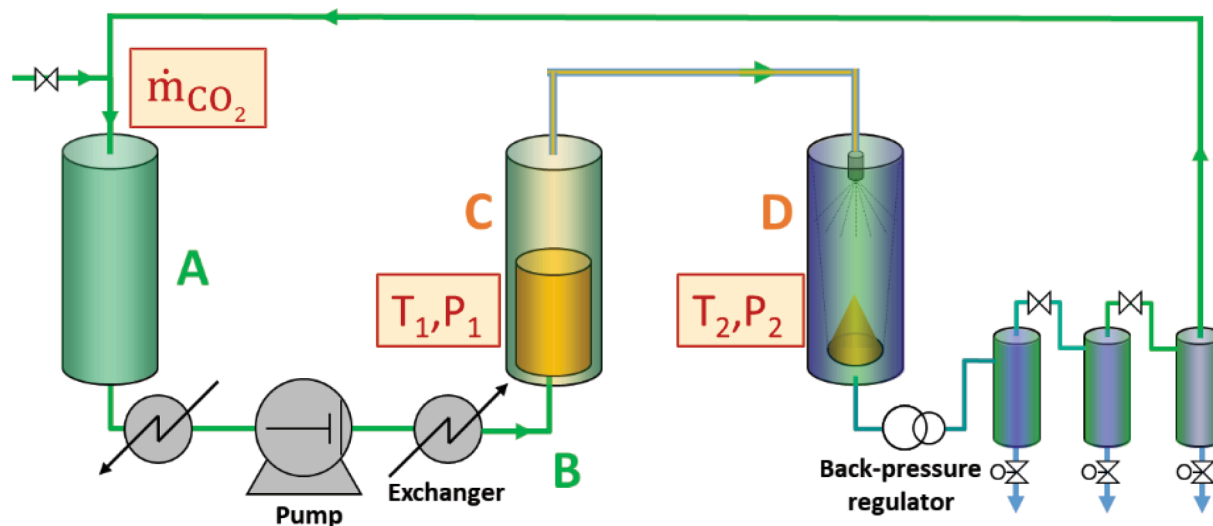


Fig. 2. Schematic representation of scCO₂ RESS apparatus. A, liquid CO₂; B, pump and thermal exchangers; C, extraction autoclave; D, crystallization autoclave.

Table 1
Operating conditions for NIF crystallization using the RESS process.

Conditions	Extraction		Crystallisation		Nozzle (μm)	^a Theoretical S	^b Theoretical driving force (kJ.mol ⁻¹)	Yield (kg _{NIF} .kg _{CO2} ⁻¹) x 10 ⁵
	T1 (K)	P1 (MPa)	T2 (K)	P2 (MPa)				
NIF P15-T33	318.15	15	333.15	5	300	43.6	4541.9	4.67
NIF P15-T53	318.15	15	353.15	5	300	10.6	3010.9	4.70
NIF P15-T73	318.15	15	373.15	5	300	2.9	1447.3	4.69
NIF P24-T33	318.15	24	333.15	5	200	134.2	5893.7	14.4
NIF P24-T53	318.15	24	353.15	5	200	32.6	4443.9	14.5
NIF P24-T73	318.15	24	373.15	5	200	9.0	2961.4	14.5
NIF P30-T33	318.15	30	333.15	5	150	314.1	6916.4	14.5
NIF P30-T53	318.15	30	353.15	5	150	76.4	5528.1	14.7
NIF P30-T73	318.15	30	373.15	5	150	21.1	4107.1	14.6

^a Retrieved from Eq. (6).

^b Retrieved from Eq. (7).

in order to check the reproducibility of measurements. The span, corresponding to particles distribution width, was calculated as follow: $Span = \frac{D_{90}-D_{10}}{D_{50}}$. Where D_x are the percentiles values that indicates the size below which x% of total particles volume was found.

2.2.5.2. Scanning electron microscopy (SEM). Scanning electron microscope (MT-3000, Hitachi, Tokyo, Japan) was used to observe the morphological shape of unprocessed and processed materials. Before analysis, samples were fixed on a SEM stub through a double-sided adhesive tape and finally plated with platinum for 100 s at 2 kV.

2.2.5.3. Differential Scanning Calorimetry (DSC). Differential Scanning Calorimetry (DSC) analysis of commercial NIF and processed samples was performed using a DSC Q200 (TA Instrument, USA). Analysed samples were placed in a non-hermetically closed aluminium pan. The analysis was carried out in a temperature range of 20 to 210 °C (293.15 to 483.15 K) at a heating rate of 5 °C/min under a dry nitrogen flow rate of 50 mL/min.

2.2.5.4. Powder X-ray diffraction (PXRD). PXRD analysis was performed using X' PERT PRO MDP, Philips PANalytical (USA) apparatus with CuK α radiation. Processed and unprocessed drug powders were stack into a sample holder. Diffractogram patterns were obtained at 45 kV, 40 mA at 2 θ in a range of 5-50° at a scanning rate of 1.228 min⁻¹.

2.2.5.5. Dissolution testing. Apparent dissolution kinetics were performed in triplicate using a USP II apparatus (AT Xtend, SOTAX, Switzerland). Tests were performed at 32 °C as required by the European Pharmacopoeia for transdermal formulations. In these experiments, diffusion cells are used. They are composed of a donor chamber where the formulation is deposited, and an acceptor compartment receiving the drug, which has permeated. Both compartments are separated by a skin membrane. The acceptor medium is filled with a medium that mimics the plasma. In order to ensure sink conditions, preliminary solubility studies in a physiological medium containing different percentages of polysorbate 20 were performed (Fig. S2). A medium containing 500 mL of serum saline solution (0.9%) with 1 wt% polysorbate 20 at 100 rpm fulfilled the set conditions. This solution is isotonic to the plasma and ensures that sink conditions are applied. For lipophilic drugs, it is usual to add the minimum amount of surfactant able to solubilize the drug (Bronaugh and Stewart, 1984; Tarnowska et al., 2019). Polysorbate 20 was chosen because it does not compromise skin membranes which are in close contact with the acceptor medium in skin absorption studies. This medium will be used in further experiments as an acceptor medium for Franz diffusions cells to follow the amount of NIF permeated over time from supersaturated solutions deposited in the donor chamber of the cell in close contact with the skin explant. For preliminary dissolution studies, twenty milligrams of processed and unprocessed drug were filled into hard-shell capsules and held to the bottom of the dissolution vessel by sinkers. Aliquots of 3 mL were

withdrawn at different time points (5, 10, 30, 60, 90, 120, 180 and 240 min), filtered through 0.45 μm mixed cellulose ester syringe filters (VWR, Fontenay-sous-Bois, France) and analysed by HPLC, as described in the previous section. The percentage of released NIF was calculated according to Eq. (5).

$$NIF_{released}(\%) = \frac{C_{NIF} \times m_{media}}{m_{initialNIF}} \times 100 \quad (5)$$

Where $m_{initialNIF}$ correspond to the mass of NIF stuffed into hard shell capsule expressed in μg . C_{NIF} is the concentration of NIF expressed in $\mu\text{g/g}$ and m_{media} the mass of dissolution media in g.

3. Results and discussion

3.1. Experimental NIF solubility in pure scCO_2

NIF solubility measurements in scCO_2 were performed at pressures ranging from 9 up to 24 MPa and at 308.15 and 318.15 K. In Table 2, CO_2 densities under different conditions of temperature and pressure from NIST Chemistry WebBook are detailed and compared to experimental data. According to the results, NIF solubility in scCO_2 increases with pressure and solvent density at a fixed temperature. Fig. 3 shows experimental solubility values compared to values from the literature (Wang et al., 2017). Overall, solubility values lower than those found in literature could be observed (Fig. 3A). However, graphical data representation showed a crossover point at 20.6 MPa equivalent to the literature (Knez et al., 1995; Wang et al., 2017). The existence of this crossover point may be explained by a higher number of carbon dioxide molecules able to interact and dissolve the solid at higher pressure for a fixed temperature. At this point, an inversion of the solubility behaviour was observed: below the crossover pressure, the density effect is preponderant. Therefore, at a given pressure, a lower temperature leads to a higher drug solubility. On the other hand, solvent behaviour changes above the crossover pressure. Indeed, the temperature has a predominant effect, meaning that a higher temperature leads to an increase of equilibrium solubility for a given pressure.

Since a large amount of data was required for the modelling application, solubility values from this study were reconciled with solubility values from the literature at this crossover point. After reconciliation of these data, very good similarities were noticed (Fig. 3B). These differences in experimental equilibrium concentration could be due to the apparatus and the assay method for the determination of the active ingredient in solution, which is particularly difficult due to its low solubility and high photodegradability.

3.2. Correlation of solubility data by Chrastil's density-based model and PR-EoS model

The Chrastil and Peng Robinson models were used to represent these

Table 2

Nifedipine solubility measurement in pure scCO_2 from 9 to 24 MPa at 308.15 and 318.15 K. SD, standard deviation of $n = 3$ experiments; N/A, $n = 1$ experiment; ρ , density was retrieved from NIST database.

T (K)	P (MPa)	Solubility	SD	Solubility	SD	ρ (kg. m^{-3})
		$w_{eqNIF} \times 10^6$ ($\text{g} \cdot \text{g}^{-1}$)	w_{eq}	$y_{eqNIF} \times 10^6$ ($\text{mol} \cdot \text{mol}^{-1}$)	y_{eq}	
308.15	9	17.21	9.32	2.19	1.18	662.13
	12	36.85	0.19	4.69	2.45	767.07
	15	67.59	6.25	8.60	0.80	815.06
	21	106.78	6.48	13.58	0.82	873.67
	24	126.49	26.40	16.09	3.35	894.88
318.15	9	6.16	6.33	0.78	0.8	337.51
	12	23.24	N/A	2.95	N/A	657.74
	15	46.76	9.44	5.95	1.20	741.97
	21	110.12	15.52	14.00	1.97	822.91
	24	145.13	N/A	18.46	N/A	849.39

data to estimate supersaturation ratios (S) for crystallization experiments. Fitting parameters of Chrastil's modelling are resumed in Table 3. It was observed that calculated parameters were similar to previous NIF Chrastil's correlation study (Wang et al., 2017). Identification of parameters leads to a ΔH^* estimation of 35.144 kJ/mol. A comparison of experimental and calculated equilibrium solubility is reported in Table 4. The results evidenced that calculated concentrations were in good agreement with experimental results. However, for temperature and pressure condition close to gas phase (318.15 K and 9 MPa), a large relative error was noticed. This model could easily be used for an extrapolation in pressure ranging the supercritical fluid region, however, there is a lack of relevance for low pressures conditions. This observation of high relative errors for density-based modelling in gas phase has been reported in various studies. It is associated with the challenge of acquiring robust experimental data (Eslamimanesh et al., 2011).

In order to obtain reliable prediction values in gaseous phase, a classical cubic equation model, the PR-EoS model, was used. This model is based on the competition of repulsive and attractive forces between the molecules in a mixture. All reconciliated data were used to fit parameters for PR-EoS model. It was noted that regardless of whether the shift was done up or down, results were more accurate than when the fitting was made on the unshifted data. As shown in Table 4, higher relative errors were observed using PR-EoS than Chrastil model over 12 MPa, confirming robustness of Chrastil's density-based model in high-pressure conditions. Moreover, the calculated crossover point of 9.5 MPa using PR-EoS showed that it was relatively distant from the experimental measurement (Fig. 4A). However, a more realistic value was calculated close to gas phase condition (318.15 K and 9 MPa) which confirms the ability of PR-EoS model to predict a wide range of conditions (Table 4). In addition, even if the crossover region was not accurate, similar isotherms profiles were observed compared to experimental values with reasonable relative errors in overall conditions (Fig. 4B and C). This model was then retained for saturation, supersaturation and driving force calculations.

3.3. Modelling application: NIF crystallization using RESS process

Crystallization processes generally refers to a supersaturation ratio (S , Eq. (6)) or driving force (Eq. (7)) to set operating conditions. Indeed, these relations describe differences between concentration and equilibrium concentration of a compound in a mixture to induce the crystallization and have an impact on its kinetics. Theoretically, high driving forces indicates faster nucleation rates than crystals growth, therefore resulting to smaller particles. In this study, supersaturation ratios were calculated from the PR-EoS model for different operating (T_1 , P_1 , T_2 and P_2) and are reported in Table 1.

$$S = \frac{f_{NIF}(T_2, P_2, y_{equil}(T_1, P_1))}{f_{NIF,eq}(T_2, P_2)} \quad (6)$$

$$\mu_{NIF}(T_2, P_2, y_{equil}(T_1, P_1)) - \mu_{NIF,eq}(T_2, P_2) = RT_2 \ln S \quad (7)$$

Calculated values showed that a high amount of drug dissolved in the extraction autoclave is required to increase the driving force. High pressures at a fixed temperature were then chosen and compared with lower ones ($y_{equil}(T_1, P_1)$) (Table 1). Selected pressures were 15, 24 and 30 MPa. The same approach was used to set conditions in the crystallization autoclave. Indeed, Fig. 5 shows NIF dependence driving force as a function of temperature, pressure, and equilibrium solubility at these conditions. This graph showed that increasing the pressure from 5 to 9 MPa inside the crystallization vessel leads to a higher driving force. Unfortunately, the process used could not achieve pressures above 5 MPa. As described in the graph, a slight impact of temperature in the crystallization vessel could be expected where a higher temperature means a lower theoretical driving force. The impact of temperature on

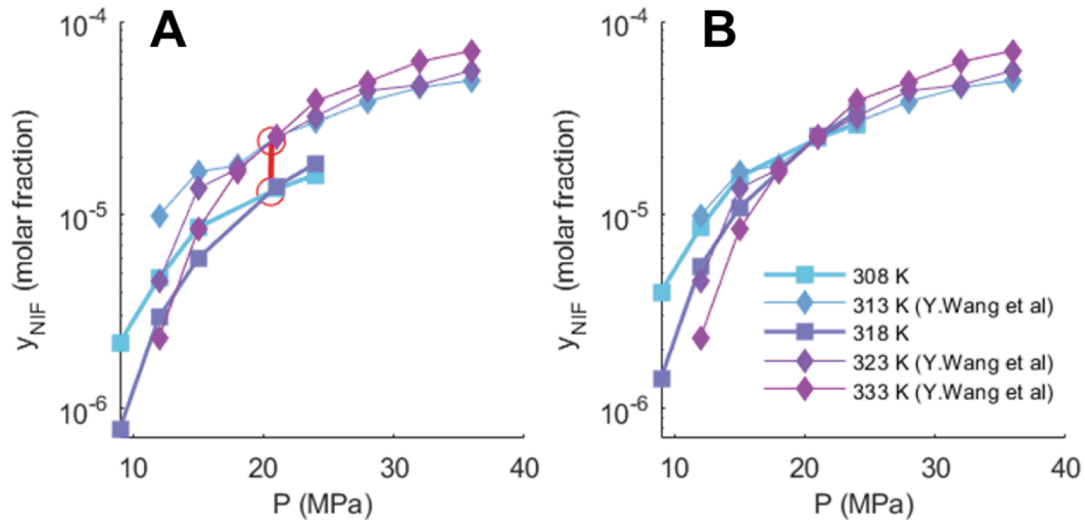


Fig. 3. Comparison of experimental NIF solubility from this study and literature. A, before reconciliation; B, after reconciliation.

Table 3

Fitting parameters obtained using Chrastil's correlation.

Parameters	a	b (K^{-1})	c	$^a f_{min}$
	6.935	- 4 227	- 44.45	0.0308

$$^a f_{min} = \frac{1}{(N_{exp} - 1)} \sqrt{\sum_{k=1}^{N_{exp}} \left(\frac{Y_{experimental,k} - Y_{calculated,k}}{Y_{experimental,k}} \right)^2}$$

yields and morphologies of powders was studied at 333.15, 353.15 and 373.15 K. All fixed conditions are reported in Table 1 and associated to corresponding supersaturation ratios and driving forces values.

3.4. Particle size

Mean diameters of a particle size distribution weighted by the volume $D[4;3]$ and of a particle size distribution weighted by the surface $D[3;2]$ are presented in Table 5 as function of operating conditions.

These mean diameters decrease as a function of the pressure in the crystallisation autoclave. For instance, for $T_2 = 353$ K, the $D[4;3]$ varied from 37 μm for raw NIF to 38, 25 and then to 9 μm for samples P15-T53, P24-T53 and P30-T53, respectively. Size reductions were also observed as a function of temperature for samples produced using 24 MPa in the extraction unit (Fig. 6). However, it was difficult to relate the size distributions obtained to supersaturation ratios alone. In fact, for the

calculation of the supersaturation ratio, it was assumed that mixtures were perfectly homogeneous in the crystallization autoclave. In this process, supersaturation will also depend on the size of the droplets created by the atomization and therefore the size of the diameter of the nozzle used. A higher expansion of the mixture occurs using smaller nozzle diameter (Sodeifian et al., 2018). Moreover, higher velocity of the jet results in higher fragmentation and, consequently, thinner droplets.

As the reduction size effect could not be only explained by supersaturation variation, it could also be explained by the expansion of gaseous CO_2 . At pressure used in the crystallization autoclave, the density of CO_2 decreases as a function of temperature, meaning less NIF- CO_2 mixture molecules for a same volume. A larger space between NIF molecules promotes nucleation in the face of crystal maturation since these ones can less easily clump together. Moreover, post-expansion temperatures at the nozzle outlet could have additional effect. Reverchon and Pallado (1996) previously modelled the significant temperature loss at the nozzle outlet. Thus, they showed that with extraction pressures of 20 and 26 MPa, temperature drop at the nozzle outlet was very high. Using outlet temperatures of 333.15 and 335.15 K, the recorded ones were below 273.15 K at the nozzle outlet. This implies a momentary phase change as the CO_2 becomes dense, even liquid, which could modify nucleation growth. Observed size reductions at 24 MPa as a function of temperature could then be related to the limitation of this momentary phase change at the nozzle outlet. At 30 MPa, a new

Table 4

Calculated from Chrastil's and Peng Robinson's models and experimental mole fraction solubility of NIF.

T (K)	P (Mpa)	$Y_{experimental}$ ($\times 10^6$)	$^a Y_{calculated}$ ($\times 10^6$)	$^a,^c$ Relative error	$^b Y_{calculated}$ ($\times 10^6$)	$^b,^c$ Relative error
308.15	24	16.1	15.9	0.01	13.2	0.18
308.15	21	13.6	13.5	0.01	8.54	0.37
308.15	15	8.60	8.34	0.03	3.92	0.54
308.15	12	4.69	5.47	0.17	2.79	0.41
308.15	9	2.19	1.97	0.10	1.89	0.14
318.15	24	18.5	17.1	0.08	22.1	0.20
318.15	21	14.0	13.7	0.02	14.9	0.06
318.15	15	5.95	6.69	0.12	7.19	0.21
318.15	12	2.95	2.90	0.02	4.78	0.62
318.15	9	0.78	2.88	2.69	1.15	0.47

^a Chrastil's model.

^b PR-EoS model.

$$^c \left(\frac{Y_{experimental,k} - Y_{calculated,k}}{Y_{experimental,k}} \right)$$

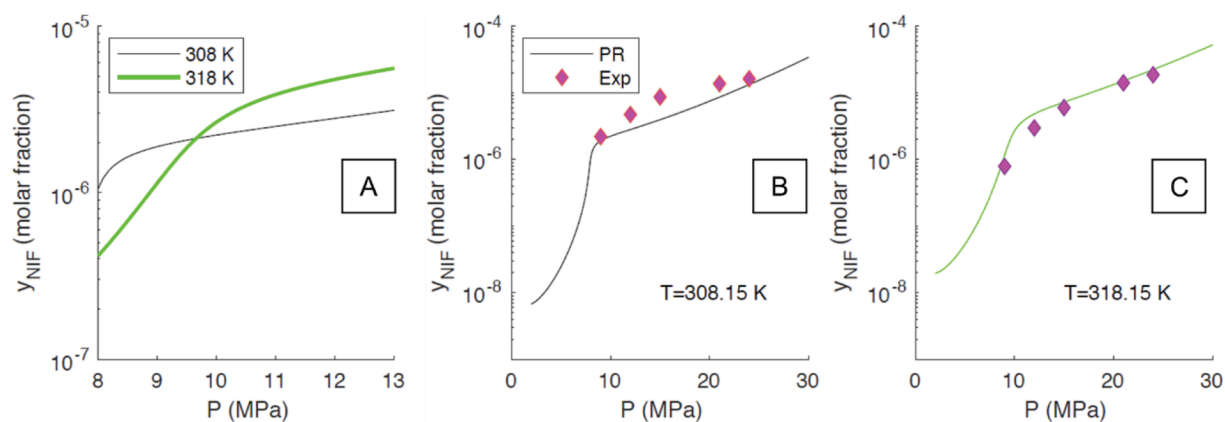


Fig. 4. Experimental and calculated solubilities with the Peng Robinson model as a function of temperature and pressure. A, crossover point evidence from modelling application; B, experimental and calculated solubilities at 308.15 K; C, experimental and calculated solubilities at 318.15 K. Optimized PR-EoS finding parameters were, $T_{c\ NIF} = 872.4\ K$, $P_{c\ NIF} = 1.933\ MPa$, $\omega_{NIF} = 0.586$, $k_{12} = 0.268$ and $l_{12} = 0.096$.

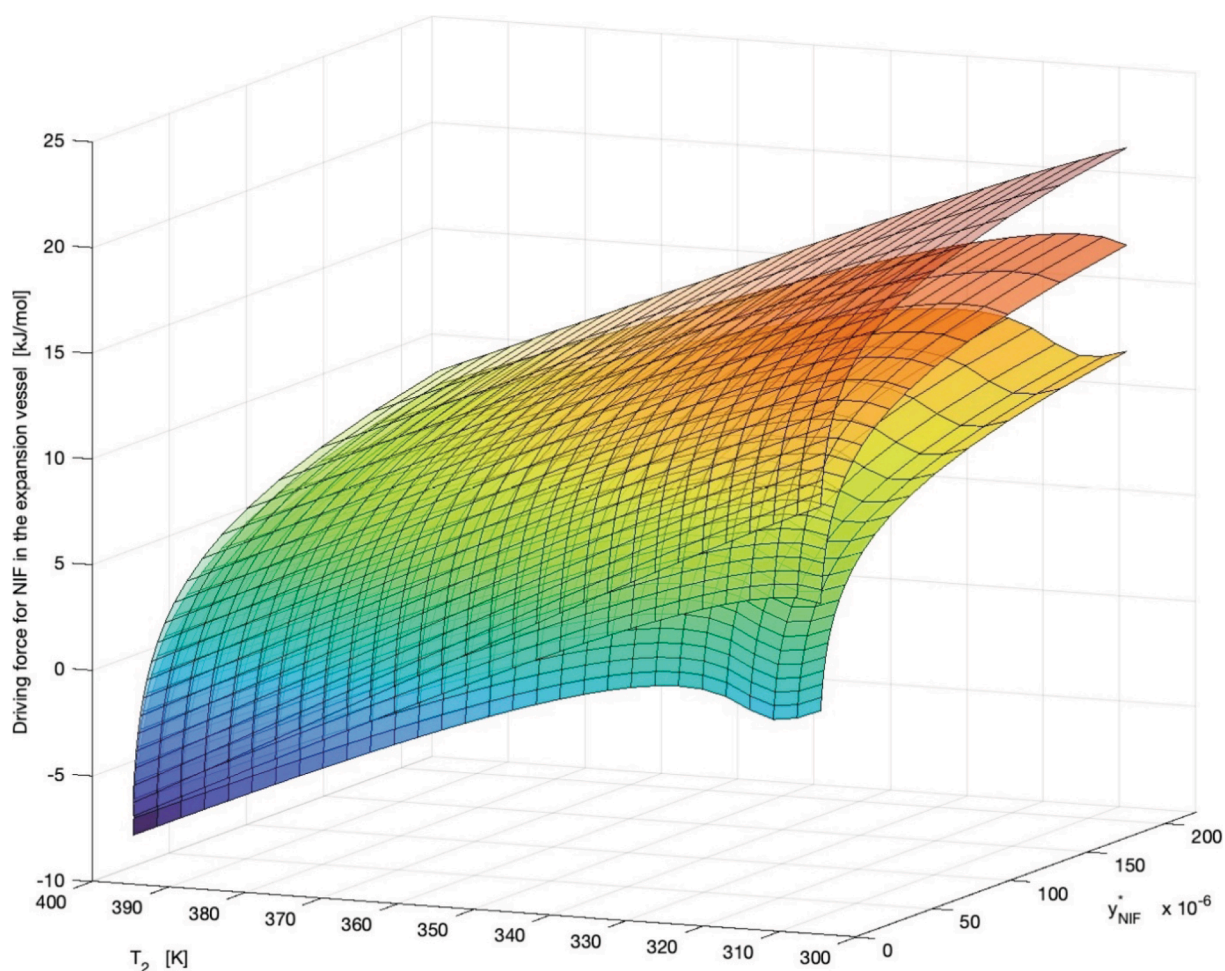


Fig. 5. Theoretical driving force represented at constant pressure (P_2) at different crystallization vessel temperatures (T_2) and correspondent equilibrium solubility of NIF in $scCO_2$. Pressures (P_2) of the three surface plots correspond from the bottom to the top to 5, 7 and 9 MPa respectively.

morphology of NIF was observed at 333.15 K in the crystallization vessel. As soon as the outlet temperature increases, this new morphology composed the whole sample (Fig. 6). An important particle size reduction was observed at these operating conditions (Table 5), indicating promising improvements for release studies. Interestingly, qualitative observation of powders obtained at 30 MPa exhibited a foamed

appearance, probably due to an increase in electrostatic repulsion as well as a lower bulk density. This lower bulk density was already described and explained by internal et external porous structure of generated NIF particles using $scCO_2$ processes (Kerč et al., 1999; Senčar-Božič et al., 1997).

Table 5
Size distribution data of raw NIF and processed NIF.

Conditions	D ₁₀ (μm)	D ₅₀ (μm)	D ₉₀ (μm)	D ₉₇ (μm)	D[4;3] (μm)	D[3;2] (μm)	Span
Raw NIF	6.7	28.0	82.1	126.5	37.8	11.6	2.7
NIF P15-T33	4.5	26.7	74.4	106.5	33.8	9.3	2.6
NIF P15-T53	6.7	35.9	74.8	92.2	38.6	12.4	1.9
NIF P15-T73	8.6	40.4	87.7	112	44.9	15.2	2.0
NIF P24-T33	5.5	25.9	60.7	80.7	30.1	10.2	2.1
NIF P24-T53	5.8	22.8	47.5	60.1	25.1	10.1	1.8
NIF P24-T73	4.7	14.9	42.1	162.5	27.0	8.6	2.5
NIF P30-T33	4.4	11.1	19.9	24.3	11.7	7.6	1.4
NIF P30-T53	1.0	2.8	9.6	73.7	9.1	2.2	3.1
NIF P30-T73	1.8	5.0	10.2	12.7	5.6	3.6	1.7

3.5. Solid state characterization

NIF crystallinity evaluation was carried out by DSC and XRPD and presented in Fig. 7 for processed samples at 24 and 30 MPa and in Fig. S3 for crystallized samples at 15 MPa. The DSC thermograms of raw NIF and crystallized NIF at 24 and 30 MPa (Fig. 7A and 7C, respectively) showed a single endothermic event at 172 °C corresponding to the melting peak of the commercial form, polymorph A (Grooff et al., 2007). Tops of the peaks seems located at a lower temperature for produced NIF compared to raw NIF. Indeed, looking at onset fusion temperatures, no significant shift could be observed (Table S1). Moreover, as bulk

densities of produced samples were lower than raw NIF, a reduced mass of powders was used for the analysis and might explain the slight shift at the top of the peaks. In addition, fusion enthalpies obtained from the DSC study for all produced samples are summarized in Table S1. These fusion enthalpies of crystallized compound correspond to raw NIF, which confirmed the crystallinity of the produced drug. According to XRPD analysis in Fig. 7B and D, Bragg peaks of A-NIF were observed, which are in accordance with literature data and were found at 2 θ degree of 8.09°, 11.75°, 16.20° (Grooff et al., 2007). DSC and XRPD analysis confirmed the crystalline nature of crystallized samples and showed no impact of scCO₂ process on drug crystallinity and polymorphic transformation.

3.6. Dissolution kinetics

Fig. 8 represents the *in vitro* release profiles of raw material and crystallized drug. A lag time of 15 min was noticed on the drug dissolution profile that is linked to hard-shell capsules dissolution and powder wettability. According to the results, an improvement of dissolution rates was observed for processed samples generated using extraction pressures of 24 and 30 MPa (Fig. 8A and B). Besides, no dissolution rate improvement was observed for powders produced at 15 MPa (data not shown). The size and specific surface of the particles, which are directly related to the dissolution rate (Noyes and Whitney, 1897), explain the lack of improvement for these samples as no reduction size was observed (Table 5). Process temperature variation in the crystallization vessel showed a slight impact on dissolution rate of crystallized NIF. Indeed, a size reduction was observed in relation to the temperature of the crystallization vessel at 24 MPa. This size reduction was well correlated to a dissolution rate improvement (Fig. 8A). Samples crystallized at 30 MPa showed faster dissolution kinetics (Fig. 8B). At 90 min, 42% was released for raw NIF against approximately 80% for crystallized NIF

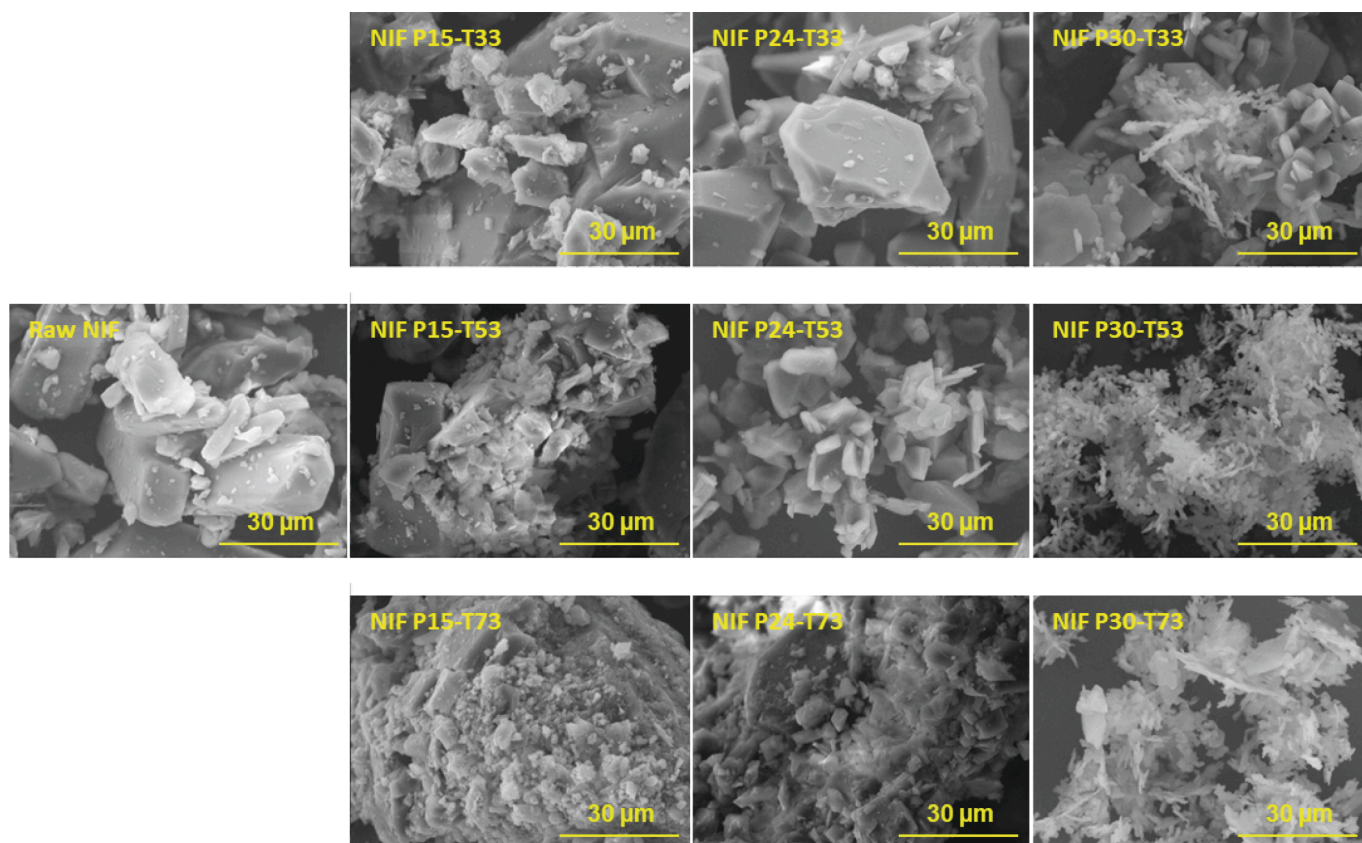


Fig. 6. SEM images of processed drug at operating conditions compared to raw NIF (magnification 2000 × ; scale bar = 30 μm).

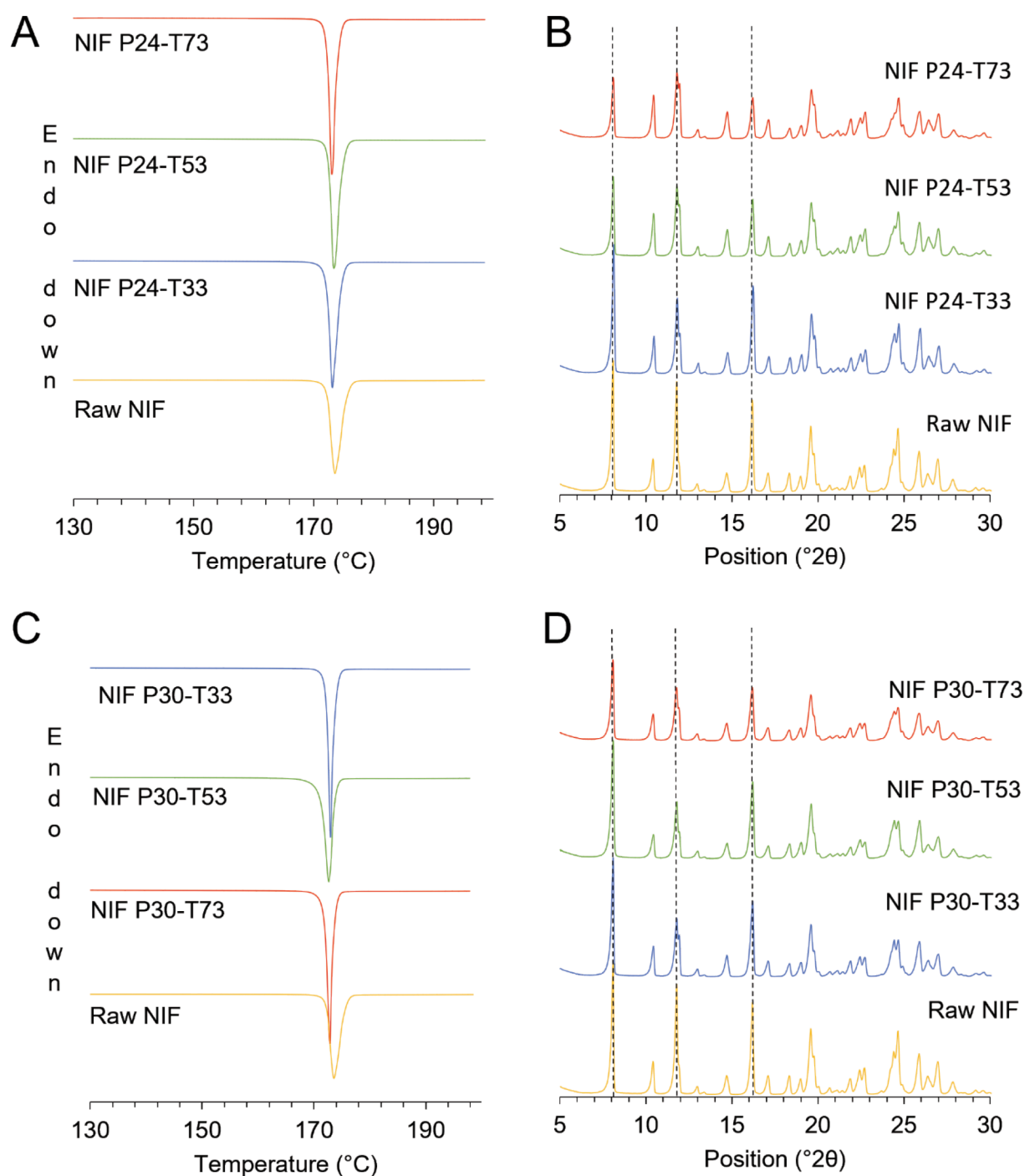


Fig. 7. DSC thermograms (A, C) and XRD diffractograms (B, D) of raw NIF and processed samples at 24 and 30 MPa respectively.

(Table S2). Other authors have also studied the dissolution profiles of micronized NIF. Senčar-Božič et al., (1997) produced micronized NIF using PGSS process, with and without additives, and showed an improvement of NIF dissolution for oral application. Nevertheless, the use of high process temperatures in this study induced NIF degradation. Sharkawi et al., (2014) investigated spray drying crystallization process of NIF, associated or not with a copolymer. They showed a reduction size of the pure crystallized NIF. Unfortunately, this size reduction did not exhibit the expected dissolution rate improvement. This behaviour was assigned to non-optimal crystallization process highlighted by physico-chemical characterizations. In contrast, co-processing NIF through spray drying using a polymeric solubilizer finally led to an improvement of dissolution rate and solubility.

Based on the results presented in this section, RESS sCO_2 process, as a solvent free technique without additives, revealed a significant improvement in NIF dissolution behaviour maintaining its physico-chemical stability.

4. Conclusion

NIF experimental solubility results in sCO_2 using a continuous flow apparatus at temperatures ($T = 308\text{--}318\text{ K}$) and pressures ($P = 9\text{--}24\text{ MPa}$), were successfully correlated with Chrastil's density-based model for supercritical fluid region but lacks relevance for lower pressures. The PR-EOS model showed more reliable estimation of solubility for lower pressures confirmed with experimental data correlation. These

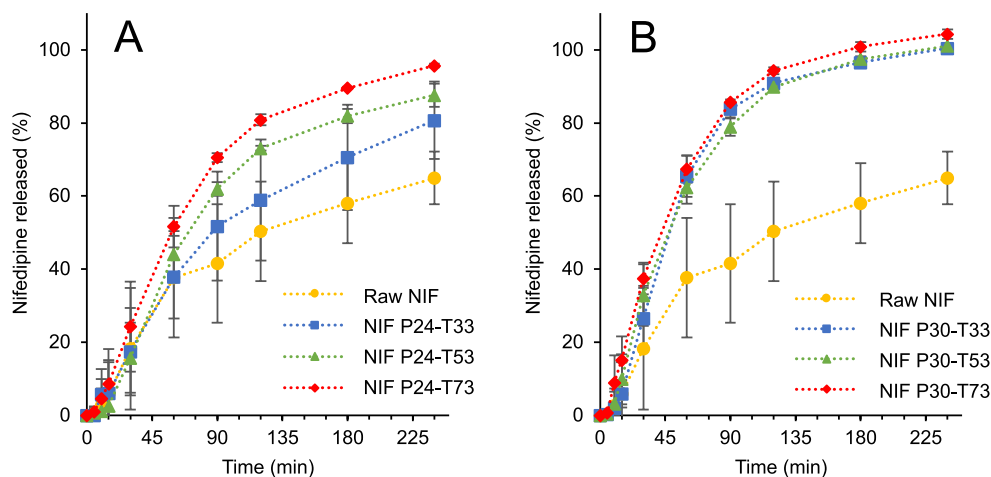


Fig. 8. Dissolution kinetics study of raw NIF and processed NIF at 24 MPa (A) and at 30 MPa (B). Error bars = SD, n = 6: 0–60 min, n = 3: 90–240 min, n = number of independent experiments.

solubility predictions allowed identifying operating conditions for the extraction and the crystallization in order to reduce NIF particles sizes. The generated particles did not show any polymorphic change and they kept the same crystalline form of NIF raw material. Finally, an improvement in dissolution kinetics was observed compared to raw NIF. This study demonstrates that the opportunities to achieve the design of an API are greater using a complete approach of particle-engineering through experimentation and thermodynamic modelling. This approach is relevant to define operating conditions and seems step forward between process development and powder properties controls of poorly water-soluble drugs (*i.e.*, size, crystallinity). In addition, the data generated in this work shows the potential of scCO₂-RESS process to improve the dissolution kinetics of NIF by reducing the particle size. The presented proposal is promising to develop a supersaturated system and also may be a suitable tool to contemplate alternative delivered through the skin.

CRediT authorship contribution statement

Thibault Massias: Conceptualization, Methodology, Investigation, Formal analysis, Writing – original draft. **Suênia de Paiva Lacerda:** Conceptualization, Formal analysis, Writing – review & editing. **Jacqueline Resende de Azevedo:** Conceptualization, Formal analysis, Writing – review & editing. **Jean-Jacques Letourneau:** Methodology, Software, Formal analysis. **Marie-Alexandrine Bolzinger:** Validation, Writing – review & editing, Supervision. **Fabienne Espalier:** Validation, Software, Writing – review & editing, Supervision.

Declaration of Competing Interest

The authors declare that they have no known competing financial interests or personal relationships that could have appeared to influence the work reported in this paper.

Data availability

Data will be made available on request.

Acknowledgements

The authors acknowledge the support of the French Ministère de l'Enseignement Supérieur et de la Recherche and the Ministère de l'Industrie.

Appendix A. Supplementary material

Supplementary data to this article can be found online at <https://doi.org/10.1016/j.ijpharm.2022.122425>.

References

- Amidon, G.L., Lennernäs, H., Shah, V.P., Crison, J.R., 1995. A theoretical basis for a biopharmaceutical drug classification: the correlation of in vitro drug product dissolution and in vivo bioavailability. *Pharm. Res. An Off J. Am. Assoc. Pharm. Sci.* 12, 413–420. <https://doi.org/10.1023/A:1016212804288>.
- Badens, E., Masmoudi, Y., Mouahid, A., Crampon, C., 2018. Current situation and perspectives in drug formulation by using supercritical fluid technology. *J. Supercrit. Fluids* 134, 274–283. <https://doi.org/10.1016/j.supflu.2017.12.038>.
- Bolten, D., Türk, M., 2012. Micronisation of carbamazepine through rapid expansion of supercritical solution (RESS). *J. Supercrit. Fluids* 62, 32–40. <https://doi.org/10.1016/j.supflu.2011.06.014>.
- Bolzinger, M.A., Briançon, S., Pelletier, J., Chevalier, Y., 2012. Penetration of drugs through skin, a complex rate-controlling membrane. *Curr. Opin. Colloid Interface Sci.* <https://doi.org/10.1016/j.cocis.2012.02.001>.
- Bronaugh, R.L., Stewart, R.F., 1984. Methods for in vitro percutaneous absorption studies III: Hydrophobic compounds. *J. Pharm. Sci.* 73, 1255–1258. <https://doi.org/10.1002/jps.2600730916>.
- Chen, B.Q., Kankala, R.K., Wang, S.B., Chen, A.Z., 2018. Continuous nanonization of lidamine by modified-rapid expansion of supercritical solution process. *J. Supercrit. Fluids* 133, 486–493. <https://doi.org/10.1016/j.supflu.2017.11.016>.
- Chrastil, J., 1982. Solubility of solids and liquids in supercritical gases. *J. Phys. Chem* 86, 3016–3021.
- Djerafi, R., Masmoudi, Y., Crampon, C., Meniai, A., Badens, E., 2015. Supercritical anti-solvent precipitation of ethyl cellulose. *J. Supercrit. Fluids* 105, 92–98. <https://doi.org/10.1016/j.supflu.2015.02.033>.
- Echizen, H., Eichelbaum, M., 1986. Clinical pharmacokinetics of verapamil, Nifedipine and Diltiazem. *Clin. Pharmacokinet.* doi: 10.2165/00003088-198611060-00002.
- Eslamimanesh, A., Mohammadi, A.H., Richon, D., 2011. Determination of sulfur content of various gases using Chrastil-type equations. *Ind. Eng. Chem. Res.* 50, 7682–7687. <https://doi.org/10.1021/ie200187v>.
- Fages, J., Lochard, H., Letourneau, J.J., Sauceau, M., Rodier, E., 2004. Particle generation for pharmaceutical applications using supercritical fluid technology. *Powder Technol.* 141, 219–226. <https://doi.org/10.1016/j.powtec.2004.02.007>.
- Fang, C.H., Chen, P.H., Chen, Y.P., Tang, M., 2020. Micronization of three active pharmaceutical ingredients using the rapid expansion of supercritical solution technology. *Chem. Eng. Technol.* 43, 1186–1193. <https://doi.org/10.1002/ceat.201900432>.
- Foster, T.S., Hamann, S.R., Richards, V.R., Bryant, P.J., Graves, D.A., McAllister, R.G., 1983. Nifedipine kinetics and bioavailability after single intravenous and oral doses in normal subjects. *J. Clin. Pharmacol.* 23, 161–170. <https://doi.org/10.1002/j.1552-4604.1983.tb02720.x>.
- Franco, P., De Marco, I., 2021. Nanoparticles and nanocrystals by supercritical CO₂-assisted techniques for pharmaceutical applications: a review. *Appl. Sci.* 11, 1–27. <https://doi.org/10.3390/app11041476>.
- Godfraind, T., 2017. Discovery and development of calcium channel blockers. *Front. Pharmacol.* <https://doi.org/10.3389/fphar.2017.00286>.
- Grooff, D., De Villiers, M.M., Liebenberg, W., 2007. Thermal methods for evaluating polymorphic transitions in nifedipine. *Thermochim. Acta* 454, 33–42. <https://doi.org/10.1016/j.tca.2006.12.009>.

- Grundey, J.S., Kherani, R., Foster, R.T., 1994. Photostability determination of commercially available nifedipine oral dosage formulations. *J. Pharm. Biomed. Anal.* 12, 1529–1535. [https://doi.org/10.1016/0731-7085\(94\)00100-6](https://doi.org/10.1016/0731-7085(94)00100-6).
- Hadgraft, J., Lane, M.E., 2016. Drug crystallization – implications for topical and transdermal delivery. *Expert Opin. Drug Deliv.* <https://doi.org/10.1517/17425247.2016.1140146>.
- Hecq, J., Deleers, M., Fanara, D., Vranckx, H., Amighi, K., 2005. Preparation and characterization of nanocrystals for solubility and dissolution rate enhancement of nifedipine. *Int. J. Pharm.* 299, 167–177. <https://doi.org/10.1016/j.ijpharm.2005.05.014>.
- Henmi, T., Fujii, M., Kikuchi, K., Yamanobe, N., Matsumoto, M., 1994. Application of an oily gel formed by hydrogenated soybean phospholipids as a percutaneous absorption-type ointment base. *Chem. Pharm. Bull. (Tokyo)*. 42, 651. <https://doi.org/10.1248/CPB.42.651>.
- Horster, F.A., 1975. Pharmacokinetics of nifedipine-14C in man. In: 2nd International Adalat® Symposium. Springer Berlin Heidelberg, pp. 124–127. doi: 10.1007/978-3-662-39666-7_16.
- Kemken, J., Ziegler, A., Müller, B.W., 1992. Influence of supersaturation on the pharmacodynamic effect of bupranolol after dermal administration using microemulsions as vehicle. *Pharm. Res. An Off. J. Am. Assoc. Pharm. Sci.* 9, 554–558. <https://doi.org/10.1023/A:1015856800653>.
- Kerč, J., Srčić, S., Knez, Z., Senčar-Božič, P., 1999. Micronization of drugs using supercritical carbon dioxide. *Int. J. Pharm.* 182, 33–39. [https://doi.org/10.1016/S0378-5173\(99\)00063-0](https://doi.org/10.1016/S0378-5173(99)00063-0).
- Khan, M.S., Roberts, M.S., 2018. Challenges and innovations of drug delivery in older age. *Adv. Drug Deliv. Rev.* <https://doi.org/10.1016/j.addr.2018.09.003>.
- Knez, Z., Škerget, M., Senčar-Božič, P., Ržner, A., 1995. Solubility of nifedipine and nifedipine in supercritical CO₂. *J. Chem. Eng. Data* 40, 216–220. <https://doi.org/10.1021/je00017a045>.
- Lagarias, J.C., Reeds, J.A., Wright, M.H., Wright, P.E., 1998. Convergence properties of the Nelder-Mead simplex method in low dimensions. *SIAM J. Optim.* 9, 112–147. <https://doi.org/10.1137/S1052623496303470>.
- Megrab, N.A., Williams, A.C., Barry, B.W., 1995. Oestradiol permeation through human skin and silastic membrane: effects of propylene glycol and supersaturation. *J. Control. Release* 36, 277–294. [https://doi.org/10.1016/0168-3659\(95\)00062-D](https://doi.org/10.1016/0168-3659(95)00062-D).
- Montes, A., Gordillo, M.D., Pereyra, C., Martínez De La Ossa, E.J., 2012. Polymer and ampicillin co-precipitation by supercritical antisolvent process. *J. Supercrit. Fluids* 63, 92–98. <https://doi.org/10.1016/j.supflu.2012.01.001>.
- Moser, K., Kriwet, K., Kalia, Y.N., Guy, R.H., 2001a. Stabilization of supersaturated solutions of a lipophilic drug for dermal delivery. *Int. J. Pharm.* 224, 169–176. [https://doi.org/10.1016/S0378-5173\(01\)00762-1](https://doi.org/10.1016/S0378-5173(01)00762-1).
- Moser, K., Kriwet, K., Naik, A., Kalia, Y.N., Guy, R.H., 2001b. Passive skin penetration enhancement and its quantification in vitro. *Eur. J. Pharm. Biopharm.* [https://doi.org/10.1016/S0939-6411\(01\)00166-7](https://doi.org/10.1016/S0939-6411(01)00166-7).
- Noyes, A.A., Whitney, W.R., 1897. The rate of solution of solid substances in their own solutions. *J. Am. Chem. Soc.* 19, 930–934. <https://doi.org/10.1021/ja02086a003>.
- Padrela, L., Rodrigues, M.A., Duarte, A., Dias, A.M.A., Braga, M.E.M., de Sousa, H.C., 2018. Supercritical carbon dioxide-based technologies for the production of drug nanoparticles/nanocrystals – a comprehensive review. *Adv. Drug Deliv. Rev.* <https://doi.org/10.1016/j.addr.2018.07.010>.
- Parhi, R., Swain, S., 2018. Transdermal evaporation drug delivery system: concept to commercial products. *Adv. Pharm. Bull.* 8, 535–550. <https://doi.org/10.15171/apb.2018.063>.
- Peng, D.Y., Robinson, D.B., 1976. A new two-constant equation of state. *Ind. Eng. Chem. Fundam.* 15, 59–64. <https://doi.org/10.1021/i160057a011>.
- Pestieau, A., Krier, F., Lebrun, P., Brouwers, A., Streeb, B., Evrard, B., 2015. Optimization of a PGSS (particles from gas saturated solutions) process for a fenofibrate lipid-based solid dispersion formulation. *Int. J. Pharm.* 485, 295–305. <https://doi.org/10.1016/j.ijpharm.2015.03.027>.
- Portero, A., Remuñán-López, C., Vila-Jato, J.L., 1998. Effect of chitosan and chitosan glutamate enhancing the dissolution properties of the poorly water soluble drug nifedipine. *Int. J. Pharm.* 175, 75–84. [https://doi.org/10.1016/S0378-5173\(98\)00245-2](https://doi.org/10.1016/S0378-5173(98)00245-2).
- Raemisch, K.D., Sommer, J., 1983. Pharmacokinetics and metabolism of nifedipine. *Hypertension* 5, 18–24. <https://doi.org/10.1161/01.hyp.5.4.pt.2.ii18>.
- Reverchon, E., Pallado, P., 1996. Hydrodynamic modeling of the RESS process. *J. Supercrit. Fluids* 9, 216–221. [https://doi.org/10.1016/S0896-8446\(96\)90051-0](https://doi.org/10.1016/S0896-8446(96)90051-0).
- Rodier, E., Lochar, H., Saucéau, M., Letourneau, J.J., Freiss, B., Fages, J., 2005. A three step supercritical process to improve the dissolution rate of Eflucimibe. *Eur. J. Pharm. Sci.* 26, 184–193. <https://doi.org/10.1016/j.ejps.2005.05.011>.
- Santos, P., Watkinson, A.C., Hadgraft, J., Lane, M.E., 2012. Influence of penetration enhancer on drug permeation from volatile formulations. *Int. J. Pharm.* 439, 260–268. <https://doi.org/10.1016/j.ijpharm.2012.09.031>.
- Saucéau, M., Fages, J., Letourneau, J.J., Richon, D., 2000. A novel apparatus for accurate measurements of solid solubilities in supercritical phases. In: *Industrial and Engineering Chemistry Research*. ACS, pp. 4609–4614. doi: 10.1021/ie000181d.
- Senčar-Božič, P., Srčić, S., Knez, Z., Kerč, J., 1997. Improvement of nifedipine dissolution characteristics using supercritical CO₂. *Int. J. Pharm.* 148, 123–130. [https://doi.org/10.1016/S0378-5173\(96\)04838-7](https://doi.org/10.1016/S0378-5173(96)04838-7).
- Sharkawi, T., Ruiz, E., Cacciaguerra, T., Domurado, M., Bataille, B., 2014. Preliminary investigation of improved solubility of nifedipine by co processing with vinylcaprolactam/vinylacetate/PEG6000 copolymer through spray dried solid dispersions. *Macromol. Symp.* 336, 47–52. <https://doi.org/10.1002/masy.201300003>.
- Sharma, A., Madhunapantula, S.V., Robertson, G.P., 2012. Toxicological considerations when creating nanoparticle-based drugs and drug delivery systems. *Expert Opin. Drug Metab. Toxicol.* <https://doi.org/10.1517/17425255.2012.637916>.
- Sodeifian, G., Sajadian, S.A., Daneshyan, S., 2018. Preparation of Aprepitant nanoparticles (efficient drug for coping with the effects of cancer treatment) by rapid expansion of supercritical solution with solid cosolvent (RESS-SC). *J. Supercrit. Fluids* 140, 72–84. <https://doi.org/10.1016/j.supflu.2018.06.009>.
- Soulaïrol, I., Tarlier, N., Bataille, B., Cacciaguerra, T., Sharkawi, T., 2015. Spray-dried solid dispersions of nifedipine and vinylcaprolactam/vinylacetate/PEG6000 for compacted oral formulations. *Int. J. Pharm.* 481, 140–147. <https://doi.org/10.1016/j.ijpharm.2015.01.012>.
- Su, C.S., Tang, M., Chen, Y.P., 2009. Micronization of nabumetone using the rapid expansion of supercritical solution (RESS) process. *J. Supercrit. Fluids* 50, 69–76. <https://doi.org/10.1016/j.supflu.2009.04.013>.
- Tarnowska, M., Briçon, S., de Azevedo, J.R., Chevalier, Y., Barratier, C., Pourcher, T., Bolzinger, M.A., 2019. Formulation of survival acceptor medium able to maintain the viability of skin explants over in vitro dermal experiments. *Int. J. Cosmet. Sci.* 41, 617–623. <https://doi.org/10.1111/ics.12581>.
- Türk, M., Bolten, D., 2016. Polymorphic properties of micronized mefenamic acid, nabumetone, paracetamol and tolbutamide produced by rapid expansion of supercritical solutions (RESS). *J. Supercrit. Fluids* 116, 239–250. <https://doi.org/10.1016/j.supflu.2016.06.001>.
- Waller, D., Renwick, A., Gruchy, B., George, C., 1984. The first pass metabolism of nifedipine in man. *Br. J. Clin. Pharmacol.* 18, 951–954. <https://doi.org/10.1111/j.1365-2125.1984.tb02569.x>.
- Wang, Y., Meng, T., Jia, D., Sun, Y., Li, N., 2017. Solubility of nifedipine and lacidipine in supercritical CO₂: measurement and correlation. *J. Solution Chem.* 46, 70–88. <https://doi.org/10.1007/s10953-016-0550-2>.
- Won, D.H., Kim, M.S., Lee, S., Park, J.S., Hwang, S.J., 2005. Improved physicochemical characteristics of felodipine solid dispersion particles by supercritical anti-solvent precipitation process. *Int. J. Pharm.* 301, 199–208. <https://doi.org/10.1016/j.ijpharm.2005.05.017>.
- Xu, J., Luo, K.Q., 2014. Enhancing the solubility and bioavailability of isoflavone by particle size reduction using a supercritical carbon dioxide-based precipitation process. *Chem. Eng. Res. Des.* 92, 2542–2549. <https://doi.org/10.1016/j.cherd.2014.03.018>.